JCTC Journal of Chemical Theory and Computation

pubs.acs.org/JCTC Article

Reconciling Accuracy and Feasibility for Barrierless Reaction Steps by the PCS/DDCI/MC-PDFT Protocol: Methane and Ethylene Dissociations as Case Studies

Luigi Crisci* and Vincenzo Barone

Cite This: J. Chem. Theory Comput. 2024, 20, 8539−8548 Read Online

ACCESS | Metrics & More | Article Recommendations | Supporting Information

ABSTRACT: Several enhancements have been introduced into state-of-the-art computational protocols for the treatment of barrierless reaction steps in the framework of variable reaction coordinate variational transition state theory. The first step is the synergistic integration of the Iterative Difference Dedicated Configuration Interaction (I-DDCI) and Pisa Composite Scheme, which defines a reduced cost, yet very accurate, computational workflow. This approach provides a near black box tool for obtaining 1D reference potentials. Then, a general strategy has been devised for tuning the level of theory used in Monte Carlo (MC) sampling, employing Multiconfiguration Pair Density Functional Theory (MC-PDFT) with dynamically adjusted Hartree−Fock exchange. Concurrently, partial geometry optimizations during the MC simulations account for the coupling between the reaction coordinates and conserved modes. The protocol closely approaches full size consistency and yields highly accurate results, with several test computations suggesting rapid convergence of the I-DDCI correction with the basis set dimensions. The capabilities of the new platform are illustrated by two case studies (the hydrogen dissociation from CH_4 and C_2H_4), which highlight its flexibility in handling different carbon hybridizations (sp^3 and sp^2). The remarkable accuracy of the computed rate constants confirms the robustness of the proposed method. Together with their intrinsic interest, these results pave the way for systematic investigations of complex gas-phase reactions through a reliable, user-friendly tool accessible to specialists and nonspecialists alike.

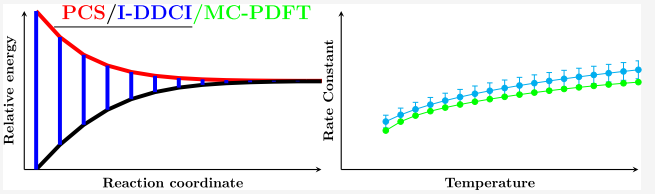

INTRODUCTION

Reactions in the gas-phase play a remarkable role in several fields of contemporary molecular sciences, ranging from astrochemistry to atmospheric chemistry and combustion, just to make a few examples. The final outcomes are tuned by the interplay of a huge number of elementary steps, which can be roughly classified into bimolecular entrance and exit channels linked by unimolecular (isomerization, tautomerization, etc.) transformations. While the unimolecular transformations are usually well described by different flavors of transition state theory (TST),[1,2] taking into account both recrossing effects (variational (V)-TST[3−6]) and nonclassical contributions (semiclassical multidimensional tunneling[7]), the situation is more involved for the entrance and exit channels, which often occur by barrierless processes. In fact, the location of dividing surfaces by one-dimensional searches along the intrinsic reaction path (RP) leading to the very successful RP-VTST model[1,5,7] becomes too restrictive. Furthermore, the different research fields are characterized by different temperature regimes and combinations of closed- and open-shell partners (not to mention charged species). In general terms, the potential energy surfaces (PES) ruling radical−molecule interactions (which are of interest mainly in astrochemistry) are well described by single-reference quantum chemical (QC) methods, whereas radical−radical interactions (the reverse of bond breaking) require multireference approaches. At the same time, tunneling effects are of utmost importance at low temperatures (again of special interest for astrochemistry), whereas the proper description of large amplitude internal motions becomes essential at high temperatures (of interest mainly in combustion processes). Based on these premises, the present work proposes an improved workflow for the computational study of the kinetics governing bond breaking elementary steps.

The Variable Reaction Coordinate Variational Transition State Theory (VRC-VTST)[8−12] can be considered the workhorse of statistical kinetics treatments for barrierless elementary steps. In the attempt of mitigating the nonrecrossing assumption, this approach requires the sampling of wide regions of flat PESs computed with sufficient accuracy.[13] Indeed, in barrierless processes, the balance between short- and long-range interactions plays a pivotal role, with this

Received: July 13, 2024
Revised: August 14, 2024
Accepted: September 4, 2024
Published: September 17, 2024

https://doi.org/10.1021/acs.jctc.4c00911
J. Chem. Theory Comput. 2024, 20, 8539−8548

requiring, in turn, flexible and accurate electronic structure approaches.[14,15]

A key ingredient of the approach is a proper account of the coupling between intermolecular librations and reaction coordinate through classical phase space sampling.[14,16,17] However, owing to its reliance on a Monte Carlo (MC) algorithm,[12] this theory is particularly prone to the evergreen computational chemists' dichotomy between feasibility and accuracy. Two main flavors of this strategy have been proposed, implemented in the Polyrate[18] and VaReCof[9] codes, respectively. In the former case, methods rooted in the Density Functional Theory (DFT) are used in the MC sampling, whereas in the second case, the sampling is performed by a minimal complete active space self-consistent field (CAS-SCF) approach. In our opinion, the most promising strategy is based on the characterization of the minimum energy dissociation path by an accurate (yet very expensive) level of theory (the high-level (HL) potential), which is then employed to correct the low-level (LL) method (either DFT or MC-SCF) employed in the MC sampling (which requires thousands of computations).[19−21] Together with this corrective potential (referred to as ΔE_{elec}), another issue is related to the use of rigid geometries (generally those of the separate fragments) in MC sampling. In this connection, a second one-dimensional corrective potential (ΔE_{geom}) can be employed, which can be obtained by geometry optimizations of the intrafragment degrees of freedom at different interfragment distances by last-generation double-hybrid functionals.[22]

In all cases, the selection of the most suitable LL method is a crucial step since, as demonstrated by Klippenstein et al., "the percent deviation in the interaction potential roughly maps to the percent deviation in the corresponding prediction of the rate constant".[23] Furthermore, 1D corrections might be inadequate to reproduce the intricate coupling between reaction coordinate, transitional (interfragment), and conserved (intrafragment) modes.[3] For instance, beyond 2000 K, the rate trend might anomalously decline to zero as interfragment separation decreases, indicating a vanishing flux minimum.[15] This limitation exemplifies the *geometrical issue*, one of the two primary constraints of the corrective approach.

Another important aspect concerns the computation of accurate ΔE_{elec} corrections, especially for regions of the PES, which require a multireference description. Generally, the internally contracted multireference configuration interaction with Davidson correction (ic-MRCI+Q)[24,25] has become the gold standard in obtaining the reference potential to calibrate the LL model. However, because of the prohibitive scaling of this approach with the dimensions of the reference space, multireference second-order perturbation theory (MR-PT2) is widely considered the method of choice.[26] In particular, the application of PT2 correction to a complete active space (CAS) wave function (CAS-PT2)[27,28] has become the most popular computational tool[29,30] because of its streamlined requirements.[26] Despite its advantages, there are some critical aspects, including the intruder state problem, usually tackled by energy shifts (real, imaginary, or IPEA),[31−34] even if, as stated by Lindh et al., "these techniques introduce a dependence of the results on a user-defined parameter".[35] Once the reference potential is obtained, calibration of a one-dimensional correction is performed, usually using a minimal (2, 2) active space or, in the case of DFT, employing the exchange and correlation functional which approaches most closely to the reference potential.[22] It should be noted here that the use of a minimal active space gives rise to the possible lack of active space consistency during the MC sampling, one of the major pitfalls of the current standard strategy.

In light of the aforementioned aspects, the main aim of the present work is to define a robust yet accurate protocol that can be applied in a nearly black box way to different reaction mechanisms. The main ingredients of the proposed strategy are as follows:

(1) The recent Pisa composite schemes (PCS)[36,37] rooted in the combined use of CCSD(T) and MP2 models for the computation of accurate energies either for single reference situations (energy minima, radical-molecule interactions) or for the high-spin (HS) states of potentially multireference low-spin (LS) wave functions (e.g., radical−radical interactions).

(2) The Iterative Difference Dedicated Configuration Interaction (I-DDCI or I-DDCI3) developed by Malrieu et al.[38,39] for computing the spin-splitting between HS and LS states in multireference regions.[23]

(3) The multiconfiguration pair density functional theory framework (MC-PDFT)[40] to calibrate the percentage of HF exchange employing the PB86 translated on-top pair density functional as a function of the interfragment distance, assuming that this parameter is the primary variable tuning the nonlocal exchange contribution during dissociation reactions.

(4) The functionals defined in point 3 for performing the MC sampling employing rigid fragment structures.

(5) The relaxation of intrafragment degrees of freedom (DOFs) during the MC sampling of interfragment DOFs in order to validate the results obtained in step 4. This step has been performed employing generalized internal coordinates (GICs)[41] and the hybrid functional best-reproducing reference revDSD-PBEP86 geometries.[42]

All these ingredients have been integrated in a user-friendly workflow, which employs the Gaussian,[43] MOLPRO,[44] and PySCF[45] codes for obtaining all the needed electronic energies. While the validation step 5 is too expensive for general use, it is performed here as a prerequisite for the planned improvement of the standard one-dimensional procedure.

The proposed strategy has been validated by two case studies, namely, the hydrogen dissociation from CH_4 and C_2H_4, which represent the two smallest prototypes of σ bond cleavage involving sp^3 and sp^2 carbon atoms. These two examples have been selected because they are well characterized from a theoretical standpoint[46−50] and, especially in the case of CH_4, several experimental[51,51−60] data are available. Furthermore, the limited dimensions of both systems permit the use of very accurate benchmark results by either Full Configuration Interaction (FCI)[61] or MRCI in its average coupled pair functional (ACPF) version[62] for both singlet and triplet electronic states. On the other hand, the latest PCS variants (which can benefit both from explicit correlation and frozen natural orbitals) have been applied to systems containing up to about 50 atoms.[37] In the same vein, the I-DDCI correction has been applied in different contexts to quite large systems since it has a small basis set dependence and allows a strong reduction of the active and virtual orbital spaces.[63−66] These aspects make the proposed strategy quite promising for systematic studies of large molecular systems of current fundamental and technological interest.

https://doi.org/10.1021/acs.jctc.4c00911
J. Chem. Theory Comput. 2024, 20, 8539−8548

METHODS

Reference Structures and Vibrational Frequencies. Optimized structure, harmonic, and anharmonic force constants of all the stationary points are obtained by double-hybrid density functionals, which provide remarkably accurate structural and spectroscopic properties at reasonable cost.[67−73] In particular, the rev-DSDPBEP86[42] functional is used in conjunction with the cc-pVTZ-F12 basis set[74] and empirical dispersion corrections estimated by the Grimme's D3 model[75] with Becke−Johnson damping (D3BJ).[76] This functional/basis set combination will be denoted as rDSD. Anharmonic zero-point energies (ZPEs) and vibrational frequencies are computed employing resonance-free expressions derived in the framework of vibrational perturbation theory to second order (VPT2).[77−81] The one-dimensional dissociation paths are determined by relaxed scans along one C−H distance. For CH_4, the rDSD method is employed, varying the bond distance from 1.08 to 5.750 Å with a step size of 0.1 Å. However, this path exhibits numerical instabilities for some distances when applied to C_2H_4. Therefore, the B3LYP functional was used in conjunction with the same basis set. The range between the equilibrium distance and 5.9 Å is covered with a step size of 0.1 Å and then extended to 9.5 Å with a step size of 0.5 Å. All the aforementioned computations are done with an unrestricted formalism employing the Gaussian package.[43]

High-Level Reference Potential. Both of the studied systems are small enough to allow for HL calculations that are generally inaccessible even for medium-sized systems. Regarding the CH_4 system, both the singlet and triplet dissociation curves are characterized at the FCI/cc-pVDZ level employing a restricted number of points (from the equilibrium distance to 3.8 Å with a step of 0.2 Å). For C_2H_4, MRCI, MRCI+Q, and MRCI/ACPF computations are performed using a full valence active space, correlating all the electrons, and employing the cc-pV5Z (hereafter 5Z) basis set.[82] The singlet−triplet energy gap is indicated as $\Delta E_{HS-LS}^{method/basis}$. Since the spin-paired singlet and the high-spin (triplet) electronic states are always well described by single-reference approaches, their energy is computed at the PCS level, which includes the following contributions:[83]

$$E(\mathrm{PCS}) = E_{V2} + \Delta E_{V} + \Delta E_{CV2} \tag{1}$$

where

$$E_{V2} = \frac{4^3 E(fc\text{-}\mathrm{MP2/4F12}) - 3^3 E(fc\text{-}\mathrm{MP2/3F12})}{4^3 - 3^3} \tag{2}$$

$$\Delta E_{V} = \frac{3^3 \Delta E(3F12) - 2^3 \Delta E(2F12)}{3^3 - 2^3} \tag{3}$$

with

$$\Delta E(n\mathrm{F12}) = E(fc\text{-}\mathrm{CCSD}(T)/n\mathrm{F12}) - E(fc\text{-}\mathrm{MP2}/n\mathrm{F12}) \tag{4}$$

and

$$\Delta E_{CV2} = E(ae\text{-}\mathrm{MP2/wC3}) - E(fc\text{-}\mathrm{MP2/wC3}) \tag{5}$$

In this context, *ae* and *fc* refer to all-electron and frozen core, respectively, while *n*F12 and wC3 denote cc-pVnZ-F12[74] and cc-pwCVTZ[84] basis sets. It is worth noting that, while several members of the PCS family employ explicitly correlated (F12) contributions,[36,37] the selected version is entirely based on conventional methods,[83] which are available in a large panel of electronic structure codes for both closed- and open-shell systems, with a negligible reduction of accuracy for reaction energies and activation barriers.

Instead of computing directly the energy of the LS electronic state, it is much more convenient to compute the energy difference (spin-splitting) between different components of the spin multiplet (in the present case, singlets and triplet). In fact, the different components have very similar dynamic correlations, which is well approximated by the PCS value for the triplet state. Then, static correlation and residual dynamic correlation can be computed accurately by dedicated difference approaches, which employ a reduced number of excitation classes.[38,39] In the present context, the Molpro software is used to perform the I-DDCI computations by combining the MRCI and MATROP modules. The initial guess for the first DDCI iteration is obtained from a state-averaged CAS-SCF computation, which includes only the two orbitals defining the spin multiplet in a minimal active space (in the present case, the open-shell singlet and the triplet). At the end of the *k*th cycle, the singlet−triplet energy gap $\Delta E_{HS-LS}^{(k)}$ is evaluated and compared to the previous one $\Delta E_{HS-LS}^{(k-1)}$. If $|\Delta E_{HS-LS}^{(k)} - \Delta E_{HS-LS}^{(k-1)}| < 1.0$ kJ mol^{-1} convergence is reached, otherwise, a state-averaged density matrix is generated and diagonalized. The number of active orbitals is then increased by one, and the procedure is repeated using as an initial guess the previously obtained state-averaged natural orbitals. This iterative/black box method yields the ΔE_{HS-LS} correction, and the final energy is calculated as follows:

$$E_{LS} = E_{HS}^{PCS} - \Delta E_{HS-LS}^{I-DDCI} \tag{6}$$

The accuracy of the ΔE_{HS-LS} values has been tested by employing the cc-pVDZ basis set for CH_4 and the 3F12 basis set for C_2H_4. Additionally, I-DDCI computations for methane were performed also in conjunction with cc-pVTZ (TZ) and cc-pVQZ (QZ) basis sets to assess the convergence of the spin-splitting correction with respect to the basis set cardinal number.

Kinetic Model. The optimized dividing surfaces are obtained differently in the long- and short-range regions of the dissociative PES. In the former zones, the dividing surface is optimized against the distance between the fragment centers of mass. For the dissociation of methane, short-range fluxes are minimized with respect to the position of two pivot points on each face of the CH_3 plane, by varying their distance from the C atom within a range of 0.01 to 2.0 a_0, with increments of 0.5 a_0, in the direction of the C_3 axis. The distance between these pivot points and the hydrogen atom is also varied, ranging from 15 to 6 a_0 with increments of 0.5 a_0, and from 6.0 to 2.75 a_0 with steps of 0.25 a_0. The long-range fluxes are optimized for the following set of distances in a_0 (20, 17, 15.5, 14.2, 13., 12.1, 11.3, 10.6, 10.0, 9.5, 8.5, 8, 7.5). Some overlap in the short- and long-range descriptions was incorporated by considering both sets of pivot points in the 8−7 a_0 region. The partial optimization is performed by the B3LYP functional in conjunction with the 6-311G(d, p) basis set, employing the unrestricted formalism, and including the D3BJ empirical dispersion correction.[76] In the following, this combination of method and basis set will be termed simply as B3. The CH bond lengths and HCH valence angles not involving the reactive hydrogen atom have been optimized for each snapshot of the MC sampling of interfragment degrees of freedom.

https://doi.org/10.1021/acs.jctc.4c00911
J. Chem. Theory Comput. 2024, 20, 8539−8548

In the ethylene case, further considerations are needed. First, both front side and back side reactions can take place (where front and back refer to the relative orientation of the H atom with respect to the C_2H_3 moiety). In principle, also hydrogen abstraction can happen, but this channel will not be considered since it is ruled by a small energy barrier.[85] We tried to discriminate between the backside and frontside, defining different regions of the sampling by means of suitable pivots (see Section 3 of the SI for further details). All the bond lengths around the reactive carbon atom and the valence angles with a C atoms as vertex (excluding in both cases parameters involving the reactive H atom) have been optimized for each structure generated in the MC sampling of interfragment degrees of freedom. In this case, all of the computations have been performed at the B3 level.

The final rate is obtained by combining the fluxes by means of the infinite potential assumption.[9,10,85,86] Nonrecrossing dynamical effects are taken into account by an empirical scaling factor of 0.9, which was derived from benchmark trajectory computations for prototypical reactions[15]

The LL energy evaluations during the Monte Carlo sampling are performed by the Gaussian package employing an "external" procedure interfaced with a compiled Python3 script that uses pySCF[45,87,88] to perform the MC-PDFT computation with the calibrated percentage of HF exchange. To minimize the overhead and latency problems, the code is compiled using the Nuitka Python compiler.[89] The VaReCof and MESS programs are used to compute the reactive fluxes and the high-pressure-limit rate constants, respectively, and the dynamical 2TS method is employed to compute the effective number of states.[90]

Calibration of the Low-Level Method. The MC-PDFT method employing the translated PB86 functional is always employed in conjunction with the DZ basis set as the LL component of the computational strategy. (2, 2) and (4, 4) active spaces are chosen for methane and ethylene, respectively. Subsequently, the HF percentage is adjusted iteratively at each point along the reaction pathway until the energy deviation from the corresponding PCS/I-DDCI reference value is less than 1.0 kJ mol^{-1}. A polynomial fit of the HF contribution as a function of the C−H distance is then carried out, and the interpolation coefficients are stored in an environment variable read by the Gaussian *external* procedure during the MC to extrapolate the HF percentage. Finally, to circumvent numerical instabilities, the asymptotic value of HF exchange is used for dividing surfaces with a C−H distance larger than the maximum value used for the calibration.

RESULTS AND DISCUSSION

Electronic Structure. *CH_3 + H.* As shown in Table 1, when employing the same DZ basis set, the I-DDCI method closely reproduces the reference FCI results, with a maximum deviation of 1.0 kJ mol^{-1} and a root-mean-square deviation (RMSD) of 0.3 kJ mol^{-1}.

To assess the convergence of the I-DDCI method with increasing basis set size, we evaluate the relative differences between the $\Delta E_{HS-LS}^{I-DDCI}$ results obtained with the cc-pVnZ basis sets,[82] with n = 2, 3, 4 (referred to in the following as DZ, TZ, and QZ, respectively) for each dissociation distance.

As shown in Figure 1, the $\Delta E_{HS-LS}^{I-DDCI}$ converges rapidly with the basis set size. The RMSD between the DZ and TZ basis sets is 2.7 kJ/mol with a maximum difference of 5.0 kJ/mol, whereas the RMSD between the TZ and QZ basis sets is only 0.9 kJ/mol with a maximum absolute difference of 1.4 kJ/mol. The complete table of these results is provided in Section 1.1 of the Supporting Information. Based on the rapid convergence with basis set size, we selected the same 3F12 basis set (which is equivalent to its QZ counterpart with additional s, p diffuse functions on C atoms, but without f functions on H and g functions on C atoms) for both the PCS and I-DDCI parts of the proposed computational protocol. The suitability of this basis set has been demonstrated in several papers[36,37] and is corroborated by the comparison between the singlet state dissociation curves obtained using the PCS/I-DDCI/3F12 and MRCI/ACPF/5Z models over a broader range of interatomic distances (Figure 2). In this case, the maximum deviation is 2.1 kJ mol^{-1}, and the RMSD is 0.1 kJ mol^{-1} (Section 1.2).

To further evaluate the robustness of the proposed protocol and identify specific regions where it might be particularly advantageous, we computed the singlet dissociation curve at the UCCSD(T)/DZ level with an electronic guess provided by CAS-SCF(2, 2) natural orbitals (see Figure 3). Compared to FCI results, UCCSD(T) computations exhibit systematic overestimation starting at 2.0 Å and significant instabilities, failing to capture the correct dissociation path. Pronounced noise is observed between 2.2 and 3.0 Å, and this erratic behavior is confirmed by T1, D1, and D2 diagnostic values in that region (Section 1.1.1). In contrast, the singlet state energy obtained by adding $\Delta E_{HS-LS}^{I-DDCI/DZ}$ to the UCCSD(T) energy of the triplet state shows excellent agreement with the FCI singlet curve (Section 1.1.2), with an RMSD of 0.3 kJ mol^{-1}.

Table 1. Shown Value is Scaled with Respect to the Asymptote Result at 10.0 Å[a]

C−H distance (Å)	ΔE_{HS-LS}^{FCI}	$\Delta E_{HS-LS}^{I-DDCI}$	difference	relative difference
1.6	504.718	505.761	−1.043	−0.2%
1.8	343.189	343.155	0.034	0.0%
2.0	223.123	223.011	0.112	0.1%
2.2	141.057	140.940	0.117	0.1%
2.4	86.711	86.633	0.078	0.1%
2.6	51.972	51.933	0.039	0.1%
2.8	30.549	30.665	−0.116	−0.4%
3.0	17.714	17.819	−0.105	−0.6%
3.2	10.168	10.256	−0.088	−0.9%
3.4	5.788	5.858	−0.071	−1.2%
3.6	3.268	3.322	−0.054	−1.6%
3.8	1.826	1.870	−0.043	−2.4%

[a]All values are in kJ mol^{-1} and the DZ basis set is always employed.

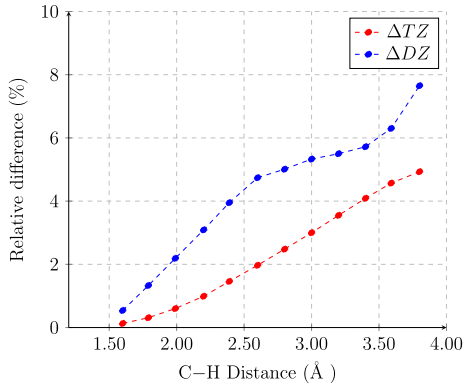

Figure 1. Relative difference between $\Delta E_{HS-LS}^{I-DDCI/nZ}$ and $\Delta E_{HS-LS}^{I-DDCI/(n+1)Z}$.

https://doi.org/10.1021/acs.jctc.4c00911
J. Chem. Theory Comput. 2024, 20, 8539−8548

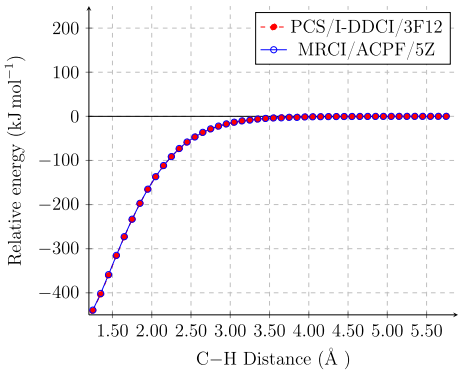

Figure 2. Relative energies with respect to the 5.75 Å asymptote.

These results indicate that a multireference treatment is not needed in all the regions of the PES describing the bond breaking but only in the intermediate zone where the low- and high-spin states are neither degenerate nor well-separated. Nonetheless, a judicious interpretation of diagnostic information can provide valuable insights into where applying the $\Delta E_{HS-LS}^{I-DDCI}$ correction is most appropriate.

CH_2CH + H. Due to the prohibitive computational cost entailed by FCI computations even using the DZ basis set, we instead employed two variants of MRCI with the 5Z basis set. Table 2 shows the singlet−triplet energy gaps computed using MRCI, MRCI+Q, MRCI/ACPF, and I-DDCI/3F12. To facilitate the comparison, all vertical excitation energies are scaled with respect to the asymptotic result at 4.9 Å, even though, as expected, the singlet−triplet gap tends to zero with an increasing interatomic distance.

The $\Delta E_{HS-LS}^{I-DDCI/3F12}$ results are close to all their multiconfigurational counterparts employing the 5Z basis, enforcing the choice of the basis set. Then, the MRCI and MRCI+Q methods show very close results throughout the dissociation process with a maximum deviation of 2.1 kJ mol^{-1}. This indicates that, as expected for small systems, the Davidson correction (+Q) does not significantly alter the energy gaps.

Table 2. Showed Value are Scaled Respect the Asymptote Result at 5.0 Å

C−H distance (Å)	ΔE_{HS-LS}^{MRCI}	$\Delta E_{HS-LS}^{MRCI+Q}$	$\Delta E_{HS-LS}^{MRCI/ACPF}$	$\Delta E_{HS-LS}^{DDCI/3F12}$
1.9	295.401	297.546	296.782	296.707
2.1	192.334	194.146	193.747	193.963
2.3	121.513	122.914	122.714	122.944
2.5	74.667	75.694	75.608	76.135
2.7	44.769	45.491	45.465	45.850
2.9	26.310	26.799	26.801	27.039
3.1	15.218	15.539	15.552	15.670
3.3	8.693	8.899	8.914	8.927
3.5	4.913	5.042	5.055	5.021
3.7	2.744	2.823	2.833	2.766
3.9	1.509	1.557	1.564	1.475
4.1	0.810	0.838	0.842	0.738
4.3	0.416	0.431	0.434	0.319
4.5	0.194	0.201	0.203	0.082
4.7	0.070	0.072	0.073	−0.053
	RMSD			
	$RMSD^{MRCI}$	$RMSD^{MRCI+Q}$	$RMSD^{MRCI/ACPF}$	
	0.840	0.283	0.211	

Nonetheless, the MRCI/ACPF method is the most reliable, since it is less prone to size inconsistency. It is, therefore, noteworthy that $RMSD^{MRCI/ACPF} < RMSD^{MRCI+Q} < RMSD^{MRCI}$. This encouraging result confirms that $\Delta E_{HS-LS}^{I-DDCI}$ (for similar geometry between singlet and triplet states) is a size-consistent correction. The above hypotheses are confirmed by comparing the singlet dissociation curves obtained with PCS/I-DDCI/3F12 and the three multiconfigurational approaches employed here (always using a 5Z basis set). The main results are summarized in Table 3.

The PCS/I-DDCI/3F12 results show a maximum RMSD of less than 1.5 kJ mol^{-1} compared to other multireference methods with the 5Z basis set, confirming the suitability of the 3F12 basis set for this protocol. Also in the case of the singlet

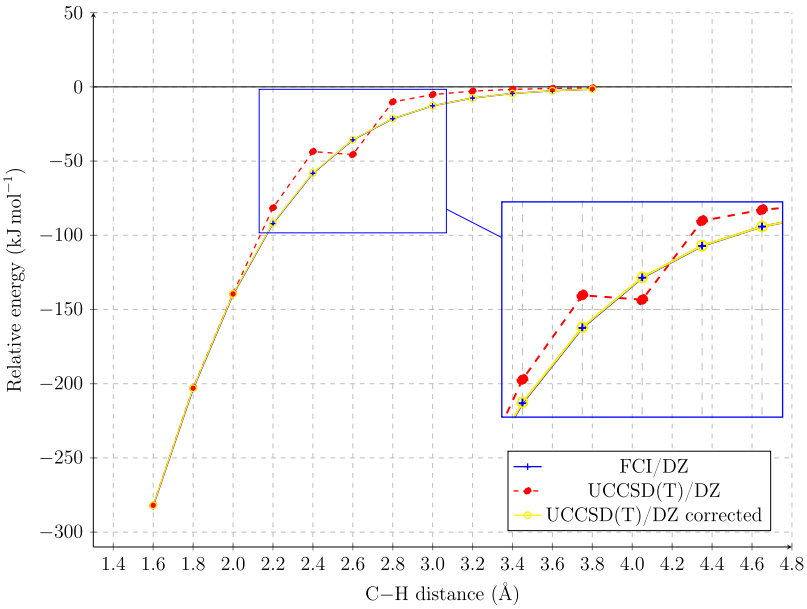

Figure 3. Comparison of the one-dimensional PES governing H dissociation from CH_4 obtained by different methods. Asymptotic value is computed at 10.0 Å.

https://doi.org/10.1021/acs.jctc.4c00911
J. Chem. Theory Comput. 2024, 20, 8539−8548

Table 3. Comparison between the Singlet Energies Obtained by MRCI/5Z, MRCI+Q/5Z, MRCI/ACPF/5Z, and PCS/I-DDCI/3F12 Computations at Different C−H Distances[a]

C−H distance (Å)	MRCI	MRCI+Q	MRCI/ACPF	PCS/I-DDCI
1.9	−204.791	−208.670	−208.848	−208.613
2.1	−143.997	−146.627	−146.837	−147.001
2.3	−98.538	−100.150	−100.351	−100.473
2.5	−66.128	−66.964	−67.126	−67.529
2.7	−43.898	−44.197	−44.311	−44.588
2.9	−29.064	−29.034	−29.104	−29.255
3.1	−19.276	−19.080	−19.118	−19.167
3.3	−12.806	−12.551	−12.570	−12.528
3.5	−8.529	−8.274	−8.282	−8.204
3.7	−5.559	−5.348	−5.350	−5.252
3.9	−3.509	−3.354	−3.353	−3.243
4.1	−2.093	−1.991	−1.990	−1.873
4.3	−1.134	−1.077	−1.076	−0.955
4.5	−0.518	−0.493	−0.492	−0.368
4.7	−0.162	−0.156	−0.155	−0.029
	RMSD			
	1.422	0.240	0.173	

[a]All energy values are given in kJ mol^{-1}.

state, the differences between MRCI and MRCI+Q do not exceed ∼4 kJ mol^{-1}, highlighting a reduced impact of the Davidson correction. Comparing the PCS/I-DDCI RMSD values listed at the bottom of Table 3, we can observe an increasing agreement with methods that incorporate size consistency. Specifically, the RMSD values for PCS/I-DDCI/3F12 relative to the MRCI, MRCI+Q, and MRCI/ACPF results are 1.422, 0.240, and 0.173 kJ mol^{-1}, respectively. This progressive reduction in RMSD values indicates that PCS/I-DDCI/3F12 can recover most of the size consistency. Finally, the reference potential, used to calibrate the percentage of HF exchange in MC-PDFT for MC sampling, is reported in Figure 4, where PCS/I-DDCI/3F12 is applied for a wider range of distances.

MC-PDFT Calibration. The optimized contribution of HF exchange against the C−H distance for both CH_4 and C_2H_4, is reported in Figure 5.

The calibrated potentials present for both cases an RMSD value of 0.2 kJ mol^{-1} with respect to the PCS/I-DDCI/3F12 one (see Tables S1 and S2). Interestingly, the contribution of HF exchange shows a similar trend for both hydrocarbons, reaching a maximum around $\sim 1.6 \cdot r_{eq}$ (where r_{eq} is the revDSD equilibrium distance of the C−H bond). Since the absolute value of the HF exchange can significantly fluctuate based on the active space and the translated on-top pair density functional, we will discuss the obtained results from a qualitative standpoint, which can give some interesting insights regarding the chemical nature of the nonlocal exchange related to the bond fission under examination. Since the core orbitals remain largely unaffected by the fission process, the nonlocal exchange gradient is closely related to the changes in the electronic layout of frontier orbitals. As the bond dissociates, the energies and occupation of the highest occupied molecular orbital (HOMO) and the lowest unoccupied molecular orbital (LUMO) become increasingly similar. This convergence is translated into greater delocalization, where the electron density is more evenly distributed across these orbitals. This requires a higher contribution of HF exchange to account for the changes in the orbital energies and the resulting delocalization.

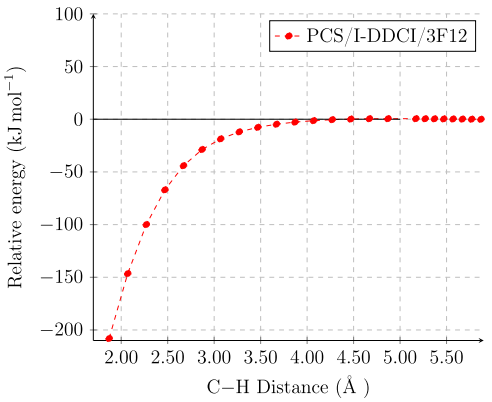

Figure 4. Singlet relative energy obtained at PCS/I-DDCI/3F12 level. Energy values are scaled with respect to the value computed at 9.5 Å.

Kinetics. In the case of hydrogen dissociation from methane, several comparisons are made to assess the quality of the rates obtained by the standard rigid MC sampling and of the enhanced version enforcing partial geometry optimizations (see Figure 6).

A corrective factor of 0.9 is applied only to the fluxes obtained by retaining rigid fragments during the Monte Carlo simulation.

The best agreement with the high-pressure-limit rates obtained by Harding et al.[15] (where CAS-PT2(2, 2)/cc-pvdz with 1-D correction is employed during the MC sampling) is provided by the method that partially optimizes those degrees of freedom associated with high-frequency modes and without the application of a dynamic factor of 0.9. This arises to compensate the discrepancy between VRC-VTST results and classical trajectory computations as well illustrated in ref 15. Specifically, a maximum discrepancy of 7% and a relative RMSD of 5% are observed. The obtained rate is slightly lower than its reference counterpart. Unfortunately, the available experimental data at temperatures around 500 and 1500 K are too widespread[91] to permit an unbiased selection between the different theoretical values. It is noteworthy that the differences are more pronounced at higher temperatures, where the impact of the coupling between intra- and interfragment degrees of freedom is more significant.

The rate constants obtained by a standard rigid fragment MC sampling show larger discrepancies but remain within an acceptable error range. The maximum deviation observed is 16%, with a relative RMSD value of 10%. This level of accuracy demonstrates that the cheaper approach neglecting partial geometry optimizations can still provide reliable results.

A noteworthy detail concerns the scaling factor; its use appears to worsen systematically all of the obtained results. Specifically, the relative RMSD of the Full Opt rate increases by 27% after application of the scaling factor. This suggests that fine-tuning the electronic potential through the proposed methodology can overcome some inherent overestimations in the standard VRC-VTST procedure, potentially leading to a more general protocol capable of yielding valuable results, even without dynamic corrective factors. Finally, as expected, the optimization of the fragments in the long-range region does

https://doi.org/10.1021/acs.jctc.4c00911
J. Chem. Theory Comput. 2024, 20, 8539−8548

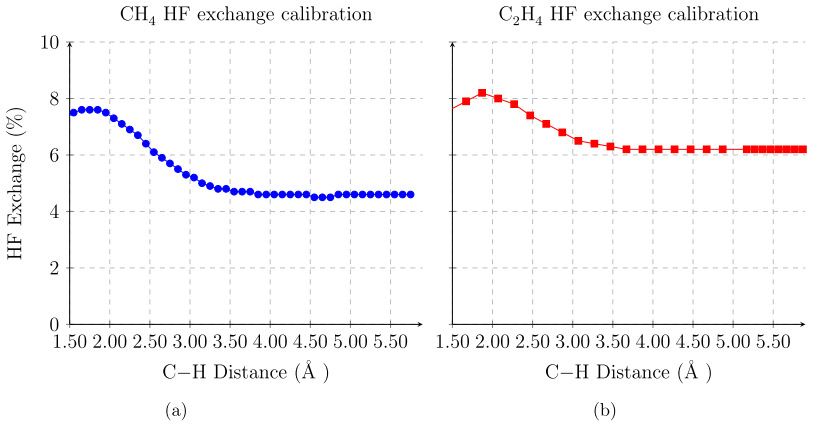

Figure 5. Comparison of two plots.

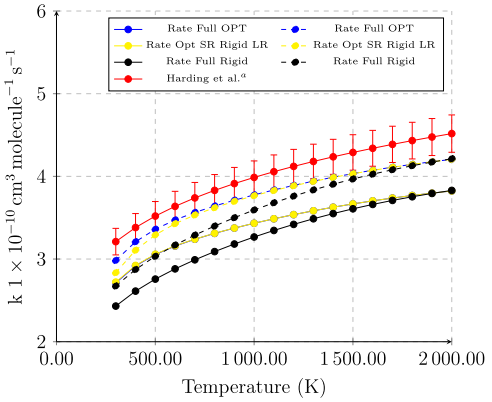

Figure 6. CH_3-H high-pressure rate constant. Dashed lines, dynamical correction factor not applied; solid lines, 0.9 dynamic correction factor applied. Full OPT stands for MC performed optimizing conserved modes for long-range and short-range samplings; Opt SR Rigid LR stands for optimization of short-range and not on long-range; and full rigid stands for MC performed maintaining a full rigid structure during all MC. [a]Rates from 1.15×10^{-10} $T^{0.18}$.[15]

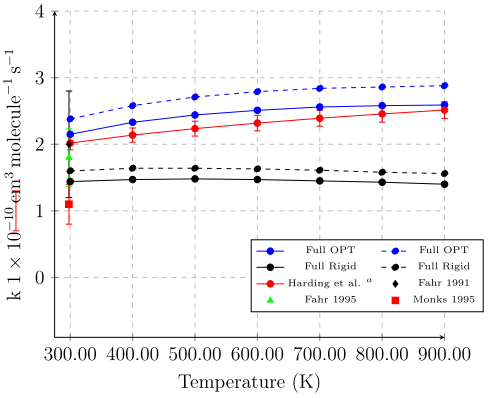

Figure 7. C_2H_3-H high-pressure rate constant. Dashed lines, dynamical correction factor not applied, solid lines 0.9 dynamic correction factor applied. Full OPT stands for MC performed optimizing conserved modes for long-range and short-range samplings, and full rigid stands for MC performed maintaining a full rigid structure during all MC. [a]Rates from 6.45×10^{-11} $T^{0.20}$.[15]

not have a significant impact, with respect to the rigid fragment sampling.

Let us now consider hydrogen dissociation from ethene.

Figure 7 compares the rate constants for C_2H_3-H recombination computed in the high-pressure limit between 300 and 1000 K by rigid and flexible MC samplings with the results obtained by Harding et al.[15] Both methods are evaluated with and without a dynamic correction factor of 0.9 dynamic correction factor. The flexible approach shows better agreement with the reference data, especially when dynamic correction. The relative differences range from 0.01 to 0.85% with the correction, compared to 1.47−4.52% without the correction, with this trend being reflected in RMSD values decreasing from 18.02 to 6.68%. The rigid approach, while reasonable, shows larger discrepancies (relative differences 8.29−21.40% with correction, 4.39−16.28% without; RMSD 38.20 and 31.58%, respectively). This systematic overestimation highlights the importance of coupling between reaction coordinates and conserved modes in the VRC-TST framework. Interestingly, both methods show good agreement with the available experimental data at 300 K, validating the overall protocol. These trends underscore the complexity of evaluating computational methods without comprehensive experimental data across a wide temperature range. Future experimental studies covering a broader temperature range would be invaluable for further validation and refinement of these approaches, potentially yielding more robust predictive tools for reaction kinetics. The overall good agreement of the proposed protocol with both theoretical benchmarks and available experimental data underscores its potential as a viable alternative in kinetic studies.

Some final remarks are in order about the general behavior of the studied reactions. To this end, the temperature dependence of the rate constants is fitted to the standard Arrhenius equation:[92]

$$K(T) = Ae^{-E_a/RT} \tag{7}$$

where A is the preexponential or frequency factor (which may involve a small dependence on temperature) and E_a is the activation energy. A more accurate fitting of the computed data is obtained by the three-parameter Arrhenius-Kooij equation,[93] largely employed in astrochemical studies.

$$K(T) = A\left(\frac{T}{300}\right)^n e^{-E/RT} \tag{8}$$

where A, n, and E are the fitting parameters and R is the universal gas constant. The above equation is based on a linear variation of the activation energy (E_a) with the temperature,

https://doi.org/10.1021/acs.jctc.4c00911
J. Chem. Theory Comput. 2024, 20, 8539−8548

($E_a/R = E + nT$), which, as we will see, is a good approximation for the considered reactions.

The Arrhenius–Kooij equation fits well the computed data, which show slightly sub- and super-Arrhenius behavior for CH_4 and C_2H_4, respectively (see Figure 8). While the

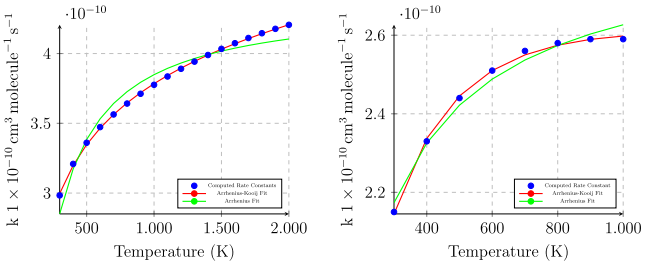

(a) Fits for CH_4 Relaxed FactorOFF (b) Fits for C_2H_4 Relaxed FactorON

Figure 8. (a)Fits for CH_4 without dynamic corrective factor and (b) Fits for C_2H_4 with dynamic corrective factor Comparison of Arrhenius and Modified Arrhenius–Kooij Fits for CH_4 and C_2H_4.

deviations from the Arrhenius behavior are not large in the considered temperature range, they show that the effective activation energy cannot be considered strictly constant. From a quantitative point of view, the Arrhenius–Kooij coefficients show that the effective activation energy is larger in the case of H dissociation from C_2H_4, possibly due to a larger energy cost involved in the deformation of valence angles around a double bond than in the umbrella motion of methyl.

H-dissociation from	Arrhenius R^2	Arrhenius-Kooij R^2
CH_4	0.992822	0.999761
C_2H_4	0.980075	0.998272

H-dissociation from	A (s^{-1})	n	E (K)
CH_4	3.3546×10^{-10}	0.1282	33.8717
C_2H_4	3.4785×10^{-10}	−0.122014	5.0175

CONCLUSIONS

The present study introduces a novel computational protocol for the treatment of barrierless reaction steps in the gas-phase by means of the variable reaction coordinate variational transition state theory. The integration of the Iterative Difference Dedicated Configuration Interaction and the Pisa Composite Scheme (PCS) leads to a near black box approach that offers a remarkable compromise between computational efficiency and high accuracy. The rapid convergence of the spin-splitting correction with the basis set dimensions, coupled with remarkable size consistency, underscores the robustness of the proposed approach. Furthermore, the MC-PDFT method with calibrated and dynamically adjusted Hartree–Fock exchange provides a reliable reduced cost engine for the Monte Carlo sampling. The robustness of the protocol is demonstrated by means of the hydrogen dissociation from CH_4 and C_2H_4, for which remarkably accurate rate constants are obtained. While further refinements are ongoing, particularly in connection with more effective samplings, the present implementation already offers a robust, user-friendly tool for both specialists and nonspecialists alike, paving the way for systematic explorations of reactions of current theoretical and experimental interest in fields ranging from combustion chemistry to astrochemistry.

ASSOCIATED CONTENT

Supporting Information

The Supporting Information is available free of charge at https://pubs.acs.org/doi/10.1021/acs.jctc.4c00911.

Additional energetic and kinetic data for the H abstraction from CH_4 and C_2H_4 and procedure for performing PCS/I-DDCI computations with the Molpro package (PDF)

AUTHOR INFORMATION

Corresponding Author

Luigi Crisci − *Scuola Normale Superiore di Pisa, I-56126 Pisa, Italy;* orcid.org/0000-0002-8140-5397; Email: luigi.crisci@sns.it

Author

Vincenzo Barone − *INSTM, 50121 Firenze, Italy;* orcid.org/0000-0001-6420-4107

Complete contact information is available at: https://pubs.acs.org/10.1021/acs.jctc.4c00911

Notes

The authors declare no competing financial interest.

ACKNOWLEDGMENTS

Funding from Gaussian Inc. is gratefully acknowledged.

REFERENCES

(1) Truhlar, D. G.; Garrett, B. C.; Klippenstein, S. J. Current Status of Transition-State Theory. *J. Phys. Chem.* **1996**, *100*, 12771–12800.
(2) Miller, W. H. Quantum Mechanical Transition State Theory and a New Semiclassical Model for Reaction Rate Constants. *J. Chem. Phys.* **1974**, *61*, 1823–1834.
(3) Zheng, J.; Zhang, S.; Truhlar, D. G. Density Functional Study of Methyl Radical Association Kinetics. *J. Phys. Chem. A* **2008**, *112*, 11509–11513.
(4) Truhlar, D. G.; Garrett, B. C. Variational Transition-State Theory. *Acc. Chem. Res.* **1980**, *13*, 440–448.
(5) Truhlar, D. G.; Garrett, B. C. Variational Transition State Theory. *Annu. Rev. Phys. Chem.* **1984**, *35*, 159–189.
(6) Meana-Pañeda, R.; Xu, X.; Ma, H.; Truhlar, D. G. Computational Kinetics by Variational Transition-State Theory with Semiclassical Multidimensional Tunneling: Direct Dynamics Rate Constants for the Abstraction of H from CH3OH by Triplet Oxygen Atoms. *J. Phys. Chem. A* **2017**, *121*, 1693–1707.
(7) Truhlar, D. G. In *Tunnelling in Molecules*; Kastner, J.; Kozuch, S., Eds.; RSC Theoretical and Computational Chemistry Series; Royal Society of Chemistry, 2021; pp 261–282.
(8) Klippenstein, S. J. A Bond Length Reaction Coordinate for Unimolecular Reactions. II. Microcanonical and Canonical Implementations with Application to the Dissociation of NCNO. *J. Chem. Phys.* **1991**, *94*, 6469–6482.
(9) Georgievskii, Y.; Klippenstein, S. J. Variable Reaction Coordinate Transition State Theory: Analytic Results and Application to the C 2 H 3+ H→ C 2 H 4 Reaction. *J. Chem. Phys.* **2003**, *118*, 5442–5455.
(10) Georgievskii, Y.; Klippenstein, S. J. Transition State Theory for Multichannel Addition Reactions: Multifaceted Dividing Surfaces. *J. Phys. Chem. A* **2003**, *107*, 9776–9781.
(11) Klippenstein, S. J. Variational Optimizations in the Rice–Ramsperger–Kassel–Marcus Theory Calculations for Unimolecular Dissociations with No Reverse Barrier. *J. Chem. Phys.* **1992**, *96*, 367–371.
(12) Klippenstein, S. J. Implementation of RRKM Theory for Highly Flexible Transition States with a Bond Length as the Reaction Coordinate. *Chem. Phys. Lett.* **1990**, *170*, 71–77.

(13) Davis, M. J.; Gray, S. K. Unimolecular Reactions and Phase Space Bottlenecks. *J. Chem. Phys.* **1986**, *84*, 5389−5411.
(14) Wardlaw, D. M.; Marcus, R. A. RRKM Reaction Rate Theory for Transition States of Any Looseness. *Chem. Phys. Lett.* **1984**, *110*, 230−234.
(15) Harding, L. B.; Georgievskii, Y.; Klippenstein, S. J. Predictive Theory for Hydrogen Atom- Hydrocarbon Radical Association Kinetics. *J. Phys. Chem. A* **2005**, *109*, 4646−4656.
(16) Marcus, R. A. Generalization of the Activated Complex Theory of Reaction Rates. II. Classical Mechanical Treatment. *J. Chem. Phys.* **1964**, *41*, 2624−2633.
(17) Marcus, R. A. Generalization of Activated-Complex Theory. III. Vibrational Adiabaticity, Separation of Variables, and a Connection with Analytical Mechanics. *J. Chem. Phys.* **1965**, *43*, 1598−1605.
(18) Zheng, J.; Bao, J. L.; Meana-Pañeda, R.; Zhang, S.; Lynch, B. J.; Corchado, J. C.; Chuang, Y. Y.; Fast, P. L.; Hu, W. P.; Liu, Y. P. et al. *Polyrate Computer Program, Version 2017-C*; Univ. Minn. Minneap: MN, 2017,.
(19) Zhang, Z. P.; Wang, S. H.; Shang, Y. L.; Liu, J. H.; Luo, S. N. Theoretical Study on Ethylamine Dissociation Reactions Using VRC-VTST and SS-QRRK Methods. *J. Phys. Chem. A* **2024**, *128*, 2191−2199.
(20) Nurkowski, D.; Klippenstein, S. J.; Georgievskii, Y.; Verdicchio, M.; Jasper, A. W.; Akroyd, J.; Mosbach, S.; Kraft, M. Ab Initio Variational Transition State Theory and Master Equation Study of the Reaction $(OH)_3SiOCH_2 + CH_3 \rightleftharpoons (OH)_3SiOC_2H_5$. *Z. Für Phys. Chem.* **2015**, *229*, 691−708.
(21) Zhou, C.-W.; Simmie, J. M.; Curran, H. J. Rate Constants for Hydrogen-Abstraction by O · H from n-Butanol. *Combust. Flame* **2011**, *158*, 726−731.
(22) Crisci, L.; Di Grande, S.; Cavallotti, C.; Barone, V. Toward an Accurate Black-Box Tool for the Kinetics of Gas-Phase Reactions Involving Barrier-less Elementary Steps. *J. Chem. Theory Comput.* **2023**, *19*, 7626−7639.
(23) Goldsmith, C. F.; Harding, L. B.; Georgievskii, Y.; Miller, J. A.; Klippenstein, S. J. Temperature and Pressure-Dependent Rate Coefficients for the Reaction of Vinyl Radical with Molecular Oxygen. *J. Phys. Chem. A* **2015**, *119*, 7766−7779.
(24) Knowles, P. J.; Werner, H.-J. Internally Contracted Multi-configuration Reference Configuration Interaction Calculations for Excited States. *Theor. Chem. Acc.* **1992**, *84*, 95−103.
(25) Werner, H.-J.; Knowles, P. J. An Efficient Internally Contracted Multiconfiguration Reference CI Method. *J. Chem. Phys.* **1988**, *89*, 5803−5814.
(26) Celani, P.; Werner, H.-J. Multireference Perturbation Theory for Large Restricted and Selected Active Space Reference Wave Functions. *J. Chem. Phys.* **2000**, *112*, 5546−5557.
(27) Dyall, K. G. The Choice of a Zeroth-order Hamiltonian for Second-order Perturbation Theory with a Complete Active Space Self-consistent-field Reference Function. *J. Chem. Phys.* **1995**, *102*, 4909−4918.
(28) Andersson, K.; Malmqvist, P.-Å.; Roos, B. O. Second-order Perturbation Theory with a Complete Active Space Self-consistent Field Reference Function. *J. Chem. Phys.* **1992**, *96*, 1218−1226.
(29) Li, H.; Chen, B.-Z.; Huang, M.-B. CASPT2 Investigation of Ethane Dissociation and Methyl Recombination Using Canonical Variational Transition State Theory. *Int. J. Chem. Kinet.* **2008**, *40*, 161−173.
(30) Coppola, F.; Nucci, M.; Marazzi, M.; Rocca, D.; Pastore, M. Norbornadiene/Quadricyclane System in the Spotlight: The Role of Rydberg States and Dynamic Electronic Correlation in a Solar-Thermal Building Block. *ChemPhotoChem* **2023**, *7*, No. e202200214.
(31) Roos, B. O.; Andersson, K.; Fülscher, M. P.; Serrano-Andrés, L.; Pierloot, K.; Merchán, M.; Molina, V. Applications of Level Shift Corrected Perturbation Theory in Electronic Spectroscopy. *J. Mol. Struct.: THEOCHEM* **1996**, *388*, 257−276.
(32) Ghigo, G.; Roos, B. O.; Malmqvist, P.-Å. A Modified Definition of the Zeroth-Order Hamiltonian in Multiconfigurational Perturbation Theory (CASPT2). *Chem. Phys. Lett.* **2004**, *396*, 142−149.
(33) Roos, B. O.; Andersson, K. Multiconfigurational Perturbation Theory with Level Shift — the Cr2 Potential Revisited. *Chem. Phys. Lett.* **1995**, *245*, 215−223.
(34) Forsberg, N.; Malmqvist, P.-Å. Multiconfiguration Perturbation Theory with Imaginary Level Shift. *Chem. Phys. Lett.* **1997**, *274*, 196−204.
(35) Battaglia, S.; Fransén, L.; Fdez Galván, I.; Lindh, R. Regularized CASPT2: An Intruder-State-Free Approach. *J. Chem. Theory Comput.* **2022**, *18*, 4814−4825.
(36) Di Grande, S.; Kallay, M.; Barone, V. Accurate Thermochemistry at Affordable Cost by Means of an Improved Version of the JunChS-F12 Model Chemistry. *J. Comput. Chem.* **2023**, *44*, 2149−2157.
(37) Di Grande, S.; Barone, V. Toward Accurate Quantum Chemical Methods for Molecules of Increasing Dimension: the New Family of Pisa Composite Schemes. *J. Phys. Chem. A* **2024**, *128*, 4886−4900.
(38) Miralles, J.; Daudey, J.-P.; Caballol, R. Variational Calculation of Small Energy Differences. *Singlet-Triplet Gap in [Cu2Cl6]2-. Chemical Physics Letters* **1992**, *198*, 555−562.
(39) Miralles, J.; Castell, O.; Caballol, R.; Malrieu, J.-P. Specific CI Calculation of Energy Differences: Transition Energies and Bond Energies. *Chem. Phys.* **1993**, *172*, 33−43.
(40) Li Manni, G.; Carlson, R. K.; Luo, S.; Ma, D.; Olsen, J.; Truhlar, D. G.; Gagliardi, L. Multiconfiguration Pair-Density Functional Theory. *J. Chem. Theory Comput.* **2014**, *10*, 3669−3680.
(41) Peng, C.; Ayala, P. Y.; Schlegel, H. B.; Frisch, M. J. Using Redundant Internal Coordinates to Optimize Equilibrium Geometries and Transition States. *J. Comput. Chem.* **1996**, *17*, 49−56.
(42) Santra, G.; Sylvetsky, N.; Martin, J. M. L. Minimally Empirical Double-Hybrid Functionals Trained against the GMTKN55 Database: revDSD-PBEP86-D4, revDOD-PBE-D4, and DOD-SCAN-D4. *J. Phys. Chem. A* **2019**, *123*, 5129−5143.
(43) Frisch, M. J.; Trucks, G. W.; Schlegel, H. B.; Scuseria, G. E.; Robb, M. A.; Cheeseman, J. R.; Scalmani, G.; Barone, V.; Petersson, G. A.; Nakatsuji, H.; Li, X. *Gaussian ~ 16 Revision C.01*, 2016.
(44) Werner, H.-J.; Knowles, P. J.; Knizia, G.; Manby, F. R.; Schütz, M.; Celani, P.; Györffy, W.; Kats, D.; Korona, T.; Lindh, R.; Mitrushenkov, A. *MOLPRO, Version, a Package of Ab Initio Programs*.
(45) Sun, Q.; et al. Recent Developments in the PySCF Program Package. *J. Chem. Phys.* **2020**, *153*, No. 024109.
(46) Golden, D. M. Yet another look at the reaction CH3 + H + M = CH4 + M. *Int. J. Chem. Kinet.* **2008**, *40*, 310−319.
(47) Miller, J. A.; Klippenstein, S. J.; Raffy, C. Solution of Some One- and Two-Dimensional Master Equation Models for Thermal Dissociation: The Dissociation of Methane in the Low-Pressure Limit. *J. Phys. Chem. A* **2002**, *106*, 4904−4913.
(48) Jasper, A. W.; Miller, J. A. Theoretical Unimolecular Kinetics for CH4 + M CH3 + H + M in Eight Baths, M = He, Ne, Ar, Kr, H2, N2, CO, and CH4. *J. Phys. Chem. A* **2011**, *115*, 6438−6455.
(49) Troe, J.; Ushakov, V. G. The Dissociation/Recombination Reaction CH4 (+M) ·CH3 + H (+M): A Case Study for Unimolecular Rate Theory. *J. Chem. Phys.* **2012**, *136*, No. 214309.
(50) Narożnik, M.; Niedzielski, J. Recombination of Radicals in the High-Pressure and High-Temperature Limit Part 2Reaction CH 3 + H. *J. Chem. Soc. Faraday Trans.* **1998**, *94*, 2541−2547.
(51) Brouard, M.; Macpherson, M. T.; Pilling, M. J. Experimental and RRKM Modeling Study of the Methyl + Hydrogen Atom and Deuterium Atom Reactions. *J. Phys. Chem.* **1989**, *93*, 4047−4059.
(52) Camilleri, P.; Marshall, R. M.; Purnell, J. H. Reaction of Hydrogen Atoms with Ethane. *J. Chem. Soc., Faraday Trans.* **1974**, *1* (70), 1434−1444.
(53) Cheng, J.-T.; Yeh, C.-T. Pressure Dependence of the Rate Constant of the Reaction Atomic Hydrogen + Methyl Radicals. Fwdarw. Methane. *J. Phys. Chem.* **1977**, *81*, 1982−1984.
(54) Cobos, C. J.; Troe, J. The Dissociation-Recombination System CH4 + M⇌ CH3 + H + M: Reevaluated Experiments from 300 to 3000 K. *Z. Für Phys. Chem.* **1990**, *167*, 129−149.
(55) Forst, W. Microcanonical Variational Theory of Radical Recombination by Inversion of Interpolated Partition Function,

https://doi.org/10.1021/acs.jctc.4c00911
J. Chem. Theory Comput. 2024, 20, 8539−8548

with Examples: Methyl + Hydrogen Atom, Methyl + Methyl. *J. Phys. Chem.* **1991**, *95*, 3612−3620.
(56) Patrick, R.; Pilling, M. J.; Rogers, G. J. A High Pressure Rate Constant for CH 3 + H and an Analysis of the Kinetics of the CH 3 + H →CH 4 Reaction. *Chem. Phys.* **1980**, *53*, 279−291.
(57) Pilling, M. J. Association Reactions of Atoms and Radicals. *Int. J. Chem. Kinet.* **1989**, *21*, 267−291.
(58) Sepehrad, A.; Marshall, R. M.; Purnell, H. Reaction between Hydrogen Atoms and Methane. *J. Chem. Soc., Faraday Trans.* **1979**, *1* (75), 835−843.
(59) Teng, L.; Jones, W. E. Kinetics of the Reactions of Hydrogen Atoms with Ethylene and Vinyl Fluoride. *J. Chem. Soc., Faraday Trans.* **1972**, *1* (68), 1267−1277.
(60) Tsang, W. Rate Constants for the Decomposition and Formation of Simple Alkanes over Extended Temperature and Pressure Ranges. *Combust. Flame* **1989**, *78*, 71−86.
(61) Knowles, P. J.; Handy, N. C. A New Determinant-Based Full Configuration Interaction Method. *Chem. Phys. Lett.* **1984**, *111*, 315−321.
(62) Gdanitz, R. J.; Ahlrichs, R. The Averaged Coupled-Pair Functional (ACPF): A Size-Extensive Modification of MR CI(SD). *Chem. Phys. Lett.* **1988**, *143*, 413−420.
(63) Barone, V.; Cacelli, I.; Ferretti, A. The Role of the Multiconfigurational Character of Nitronyl-Nitroxide in the Singlet−Triplet Energy Gap of Its Diradicals. *Phys. Chem. Chem. Phys.* **2018**, *20*, 18547−18555.
(64) Jung, J.; Guennic, B. L.; Fedin, M. V.; Ovcharenko, V. I.; Calzado, C. J. Mechanism of Magnetostructural Transitions in Copper-Nitroxide-Based Switchable Molecular Magnets: Insights from Ab Initio Quantum Chemistry Calculations. *Inorg. Chem.* **2015**, *54*, 6891−6899.
(65) Barone, V.; Boilleau, C.; Cacelli, I.; Ferretti, A.; Monti, S.; Prampolini, G. Structure−Properties Relationships in Triplet Ground State Organic Diradicals: A Computational Study. *J. Chem. Theory Comput.* **2013**, *9*, 300−307.
(66) Barone, V.; Cacelli, I.; Ferretti, A.; Monti, S.; Prampolini, G. Singlet−Triplet Energy Gap of a Diarylnitroxide Diradical by an Accurate Many-Body Perturbative Approach. *Phys. Chem. Chem. Phys.* **2011**, *13*, 4709−4714.
(67) Santra, G.; Martin, J. M. L. Do Double-Hybrid Functionals Benefit from Regularization in the PT2 Term? Observations from an Extensive Benchmark. *J. Phys. Chem. Lett.* **2022**, *13*, 3499−3506.
(68) Biczysko, M.; Panek, P.; Scalmani, G.; Bloino, J.; Barone, V. Harmonic and Anharmonic Vibrational Frequency Calculations with the Double-Hybrid B2PLYP Method: Analytic Second Derivatives and Benchmark Studies. *J. Chem. Theory Comput.* **2010**, *6*, 2115−2125.
(69) Goerigk, L.; Grimme, S. Double-Hybrid Density Functionals. *WIREs Comput. Mol. Sci.* **2014**, *4*, 576−600.
(70) Graham, D. C.; Menon, A. S.; Goerigk, L.; Grimme, S.; Radom, L. Optimization and Basis-Set Dependence of a Restricted-Open-Shell Form of B2-PLYP Double-Hybrid Density Functional Theory. *J. Phys. Chem. A* **2009**, *113*, 9861−9873.
(71) Mehta, N.; Casanova-Páez, M.; Goerigk, L. Semi-Empirical or Non-Empirical Double-Hybrid Density Functionals: Which Are More Robust? *Phys. Chem. Chem. Phys.* **2018**, *20*, 23175−23194.
(72) Sancho-García, J. C.; Adamo, C. Double-Hybrid Density Functionals: Merging Wavefunction and Density Approaches to Get the Best of Both Worlds. *Phys. Chem. Chem. Phys.* **2013**, *15*, 14581−14594.
(73) Penocchio, E.; Piccardo, M.; Barone, V. Semiexperimental Equilibrium Structures for Building Blocks of Organic and Biological Molecules: The B2PLYP Route. *J. Chem. Theory Comput.* **2015**, *11*, 4689−4707.
(74) Peterson, K. A.; Adler, T. B.; Werner, H.-J. Systematically Convergent Basis Sets for Explicitly Correlated Wavefunctions: The Atoms H, He, B−Ne, and Al−Ar. *J. Chem. Phys.* **2008**, *128*, No. 084102.
(75) Grimme, S.; Antony, J.; Ehrlich, S.; Krieg, H. A Consistent and Accurate Ab Initio Parametrization of Density Functional Dispersion Correction (DFT-D) for the 94 Elements H-Pu. *J. Chem. Phys.* **2010**, *132*, No. 154104.
(76) Grimme, S.; Ehrlich, S.; Goerigk, L. Effect of the Damping Function in Dispersion Corrected Density Functional Theory. *J. Comput. Chem.* **2011**, *32*, 1456−1465.
(77) Papousek, D. D.; Aliev, M. R. M. R. *Molecular Vibrational-Rotational Spectra*; Studies in Physical and Theoretical Chemistry; Elsevier: Amsterdam, 1982.
(78) Barone, V. Anharmonic Vibrational Properties by a Fully Automated Second-Order Perturbative Approach. *J. Chem. Phys.* **2004**, *122*, No. 014108.
(79) Bloino, J.; Biczysko, M.; Barone, V. General Perturbative Approach for Spectroscopy, Thermodynamics, and Kinetics: Methodological Background and Benchmark Studies. *J. Chem. Theory Comput.* **2012**, *8*, 1015−1036.
(80) Schuurman, M. S.; Allen, W. D.; von Ragué Schleyer, P.; Schaefer, H. F., III The Highly Anharmonic BH5 Potential Energy Surface Characterized in the Ab Initio Limit. *J. Chem. Phys.* **2005**, *122*, No. 104302.
(81) Truhlar, D. G. A Simple Approximation for the Vibrational Partition Function of a Hindered Internal Rotation. *J. Comput. Chem.* **1991**, *12*, 266−270.
(82) Dunning, T. H. Gaussian Basis Sets for Use in Correlated Molecular Calculations. I. The Atoms Boron Through Neon and Hydrogen. *J. Chem. Phys.* **1989**, *90*, 1007−1023.
(83) Barone, V.; Crisci, L.; Di Grande, S. Accurate Thermochemical and Kinetic Parameters at Affordable Cost by Means of the Pisa Composite Scheme (PCS). *J. Chem. Theory Comput.* **2023**, *19*, 7273−7286.
(84) Peterson, K. A.; Dunning, T. H., Jr Accurate Correlation Consistent Basis Sets for Molecular Core−Valence Correlation Effects: The Second Row Atoms Al−Ar, and the First Row Atoms B−Ne Revisited. *J. Chem. Phys.* **2002**, *117*, 10548−10560.
(85) Klippenstein, S. J.; Harding, L. B. A Theoretical Study of the Kinetics of C2H3+H. *Phys. Chem. Chem. Phys.* **1999**, *1*, 989−997.
(86) Harding, L. B.; Klippenstein, S. J. Theoretical Kinetic Estimates for the Recombination of Hydrogen Atoms with Propargyl and Allyl Radicals. *Proceedings of the Combustion Institute* **2000**, *28*, 1503−1509.
(87) Sun, Q.; Berkelbach, T. C.; Blunt, N. S.; Booth, G. H.; Guo, S.; Li, Z.; Liu, J.; McClain, J. D.; Sayfutyarova, E. R.; Sharma, S.; Wouters.; et al. PySCF: The Python-based Simulations of Chemistry Framework. *WIREs Comput. Mol. Sci.* **2018**, *8*, No. e1340.
(88) Sun, Q. Libcint: An Efficient General Integral Library for Gaussian Basis Functions. *J. Comput. Chem.* **2015**, *36*, 1664−1671.
(89) Nuitka/Nuitka. Nuitka Organization, 2024.
(90) Georgievskii, Y.; Miller, J. A.; Burke, M. P.; Klippenstein, S. J. Reformulation and Solution of the Master Equation for Multiple-Well Chemical Reactions. *J. Phys. Chem. A* **2013**, *117*, 12146−12154.
(91) Su, M.-C.; Michael, J. C2D5I dissociation and D+ CH3→ CH2D+ H at high temperature: Implications to the high-pressure rate constant for CH4 dissociation. *Proceedings of the Combustion Institute* **2002**, *29*, 1219−1227.
(92) Laidler, K. J. A Glossary of Terms Used in Chemical Kinetics, Includin Reaction Dynamics (IUPAC Recommendations 1996). *Pure Appl. Chem.* **1996**, *68*, 149−192.
(93) Kooij, D. M. Über die Zersetzung des gasförmigen Phosphorwasserstoffs. *Z. Phys. Chem.* **1893**, *120*, 155−161.

https://doi.org/10.1021/acs.jctc.4c00911
J. Chem. Theory Comput. 2024, 20, 8539−8548